COMMUNICATIONS IN COMPUTATIONAL PHYSICS
Vol. **5**, No. 2-4, pp. 426-441

Commun. Comput. Phys.
February 2009

Spectral Elliptic Solvers in a Finite Cylinder

F. Auteri* and L. Quartapelle

Politecnico di Milano, Via La Masa 34, 20156 Milano, Italy.

Received 7 August 2007; Accepted (in revised version) 22 February 2008

Available online 1 August 2008

Abstract. New direct spectral solvers for the 3D Helmholtz equation in a finite cylindrical region are presented. A purely variational (no collocation) formulation of the problem is adopted, based on Fourier series expansion of the angular dependence and Legendre polynomials for the axial dependence. A new Jacobi basis is proposed for the radial direction overcoming the main disadvantages of previously developed bases for the Dirichlet problem. Nonhomogeneous Dirichlet boundary conditions are enforced by a discrete lifting and the vector problem is solved by means of a classical uncoupling technique. In the considered formulation, boundary conditions on the axis of the cylindrical domain are never mentioned, by construction. The solution algorithms for the scalar equations are based on double diagonalization along the radial and axial directions. The spectral accuracy of the proposed algorithms is verified by numerical tests.

AMS subject classifications: 65N30, 65N35

Key words: Spectral elliptic solvers, Dirichlet and Neumann conditions, cylindrical coordinates, Legendre and Jacobi polynomials, uncoupled vector problem.

1 Introduction

Several problems in physics and engineering involve the solution of elliptic problems in cylindrical coordinates. Among the numerical techniques proposed so far are finite differences, spectral methods and spectral element methods. This work is concerned with spectral approximations. For a comprehensive theoretical framework see the monograph by Bernardi, Dauge and Maday [5].

The main difficulty with cylindrical coordinates lies in the axis singularity, the so-called 'pole' or 'centre problem'. However, the pole problem does not represent a true difficulty and can be actually turned into an opportunity when discretizing the equation. In fact, the Fourier components $u_m(r,z)$ of a scalar function $u(r,z,\phi)$ of the cylindrical

*Corresponding author. *Email address:* auteri@aero.polimi.it (F. Auteri)

coordinates (r,z,ϕ) must satisfy the following conditions to be a regular function of $\mathbb{R}^3$ [12]

$$u_m(r,z) = r^{|m|} U_m(r^2,z),$$

with function $U_m(s,z)$, $s \geq 0$, being a regular function of its two variables. If such conditions are not satisfied, the pole problem arises, since the numerical scheme provides an unwanted over-resolution near the cylinder axis which can severely limit the time step when time dependent problems have to be solved. On the other hand, the regularity conditions are helpful since they can be exploited to reduce the number of basis functions employed, by omitting the functions not satisfying them.

Several spectral methods have been proposed in the past in an attempt to satisfy the aforementioned regularity conditions [7]. In some cases, they are fulfilled only partially, as is the case, for instance, of shifted Chebyshev polynomials of quadratic argument, where the parity condition is satisfied, or Legendre-Galerkin, Chebyshev-Galerkin and Chebyshev-Legendre-Galerkin methods proposed by Shen and his co-workers [13,14,19], where just the essential conditions with the Helmholtz are satisfied. Bessel functions and polar Robert functions [16] satisfy all the conditions, but the former provide only algebraic convergence and the latter are severely ill conditioned. Other kinds of spectral approximations were proposed that disregarded completely the centre problem, such as tau-Chebyshev methods, see, e.g., [8] and Galerkin-Legendre collocation methods [6,17]. For instance, a direct spectral collocation method for the Poisson equation in polar and cylindrical coordinates has been proposed [9].

The first well conditioned basis that satisfies all the regularity conditions and provides spectral accuracy has been proposed by Matsushima and Marcus [15] in the context of the solution of 2D Neumann boundary value problems, see also Verkley [20]. Unfortunately, the condition numbers associated with Helmholtz operator grow as the fourth power of the degree for this basis. Moreover, its application to solve homogeneous and nonhomogeneous Dirichlet problems is unduly complicated.

This paper describes new direct spectral solvers for 3D scalar and vector elliptic equations supplemented by Dirichlet boundary conditions in a cylinder of finite axial extent. The solution algorithms are all based on a Galerkin variational formulation of the elliptic boundary value problem so that there is no need to introduce the idea of collocation. After the Fourier representation of the angular dependence, the spectral approximation of the unknown coefficients in the azimuthal plane is achieved by means of a new one-sided Jacobi polynomial basis for the radial variable and by bases of Legendre polynomials for the axial variable. A distinctive feature of the proposed 3D solvers is that the size of discrete subspaces associated with the radial operators is lower at higher Fourier wavenumbers.

In the case of the vector problem, the classical uncoupling of the radial and azimuthal components is employed. The uncoupling transformation is used in conjunction with the new Jacobi representation of variable size to implicitly satisfy all of the regularity conditions for the vector problem—a result which, to the best of our knowledge, is new.

All the proposed spectral solvers rely upon the double diagonalization of the discrete operators in the radial and axial directions. Numerical comparisons are given to assess the spectral accuracy of the proposed direct solvers.

2 Scalar Helmholtz equation in cylindrical coordinates

Let us consider the Helmholtz equation in cylindrical coordinates with unknown $u = u(r,z,\phi)$, in the cylindrical domain of finite axial extent $\Omega \equiv (0,c]\times[-H,H]\times[0,2\pi)$, which includes part of the axis,

$$-\frac{1}{r}\frac{\partial}{\partial r}\left(r\frac{\partial u}{\partial r}\right)-\frac{1}{r^2}\frac{\partial^2 u}{\partial \phi^2}-\frac{\partial^2 u}{\partial z^2}+\gamma u = f(r,z,\phi). \tag{2.1}$$

where γ is a non-negative constant, $f(r,z,\phi)$ is a known source term defined in a cylindrical domain. Thanks to the periodic character of the ϕ variable, the right-hand side and the unknown can be expanded by means of a real Fourier series. In order to discretize the problem, the series is truncated at a suitable integer $M>0$, so that $-M+1\le m\le M$, and the Fourier expansions are approximated by finite summations; for instance, the truncated expansion of the unknown is

$$u(r,z,\phi) = u_0(r,z)+2\sum_{m=1}^{M-1}\Big[u_m(r,z)\cos(m\phi)-u_{-m}(r,z)\sin(m\phi)\Big]+u_M(r,z)\cos(M\phi), \tag{2.2}$$

where the coefficients $u_m(r,z)$ and $u_{-m}(r,z)$, for $m=0,1,2,\cdots$, are defined by

$$u_{\pm m}(r,z) = \frac{1}{2\pi}\int_0^{2\pi} u(r,z,\phi)\begin{matrix}\cos(m\phi)\\ \sin(m\phi)\end{matrix} d\phi. \tag{2.3}$$

The absence of the coefficient 2 in front of last term in (2.2) should be noticed. A similar Fourier expansion is used for the right-hand side f.

The expansions can now be introduced in the original differential equation (2.1). Equating similar terms and simplifying, we obtain a system of uncoupled equations. To obtain the variational form in the proper weighted Sobolev space, each equation is multiplied by r. Introducing the dimensionless variables $\rho = r/c$ and $\zeta = z/H$, $0<\rho\le 1$ and $-1\le\zeta\le 1$, and recasting in weak form by the Galerkin method, the elliptic equation for the transformed unknown $\tilde{u}_m(\rho,\zeta) = u_m(r,z)$, which will still be indicated by the same letter u_m, as $u_m(\rho,\zeta)$, is obtained

$$\begin{aligned}
&\int_0^1\int_{-1}^1\left[\frac{\rho}{c^2}\frac{\partial v}{\partial\rho}\frac{\partial u_m}{\partial\rho}+\frac{m^2}{c^2}\frac{v u_m}{\rho}+\gamma\rho v u_m+\rho\frac{\partial v}{\partial\zeta}\frac{\partial u_m}{\partial\zeta}\frac{1}{H^2}\right]d\rho d\zeta\\
&\quad=\int_0^1\int_{-1}^1\rho v(\rho,\zeta)f_m(c\rho,H\zeta)\,d\rho d\zeta+\frac{1}{c^2}\int_{-1}^1 v(1,\zeta)\frac{\partial u_m(1,\zeta)}{\partial\rho}d\zeta\\
&\qquad-\frac{1}{H^2}\int_0^1\rho v(\rho,-1)\frac{\partial u_m(\rho,-1)}{\partial\zeta}d\rho+\frac{1}{H^2}\int_0^1\rho v(\rho,1)\frac{\partial u_m(\rho,1)}{\partial\zeta}d\rho,
\end{aligned} \tag{2.4}$$

where $v(\rho,\zeta)$ denotes the weighting function. To ensure infinite differentiability of the solution on the axis, the Fourier components $u_m(\rho,\zeta)$ will have to satisfy the regularity conditions for $\rho\to 0$ reported in [12]:

$$u_m(\rho,\zeta)\sim\rho^{|m|}U_m(\rho^2,\zeta),$$

where U_m is a regular function.

3 Neumann solver using the Matsushima and Marcus basis

Let us first consider the case of Neumann boundary conditions on the entire surface of the cylindrical region:

$$\frac{\partial u}{\partial n}\Big|_{\partial\Omega}=b, \tag{3.1}$$

where b is the boundary datum defined on cylinder boundary $\partial\Omega$. When $\gamma=0$, the solution is determined up to an additive constant provided the right-hand side satisfies the compatibility condition $\int_\Omega f=-\int_{\partial\Omega}b$.

The Neumann boundary conditions for the Fourier coefficients $u_m(r,z)$ of the solution, defined in the rectangle $\omega\equiv(0,c]\times[-H,H]$, are

$$\frac{\partial u_m(c,z)}{\partial r}=b_m^{\mathrm{o}}(z),\ \ |z|\le H,\qquad \frac{\partial u_m(r,\mp H)}{\partial z}=b_m^{\mathrm{b,t}}(r),\ \ 0<r\le c. \tag{3.2}$$

Taking into account the Neumann boundary conditions for the transformed unknown $u_m(\rho,\zeta)$, the weak equation (2.4) is modified by replacing all boundary terms with those including the boundary values, namely,

$$\frac{1}{c}\int_{-1}^{1}v(1,\zeta)b_m^{\mathrm{o}}(H\zeta)\,d\zeta-\frac{1}{H}\int_0^1\rho v(\rho,-1)b_m^{\mathrm{b}}(c\rho)\,d\rho+\frac{1}{H}\int_0^1\rho v(\rho,1)b_m^{\mathrm{t}}(c\rho)\,d\rho. \tag{3.3}$$

To satisfy the aforementioned regularity conditions in an optimal way and to avoid any over-resolution near the axis, we can approximate $u_m(\rho,\zeta)$ employing the basis proposed for the radial direction in polar coordinates by Matsushima and Marcus [15], see also [20]. Then, the approximation to $u_m(\rho,\zeta)$ is expressed by the following double expansion

$$u_{\pm m}(\rho,\zeta)=\sum_{k=0}^{M-m}\rho^m\hat{P}_k^{(0,m)}\left(2\rho^2-1\right)\hat{u}_{k;j;\pm m}\hat{L}_j(\zeta)\sum_{j=0}^{J}, \tag{3.4}$$

where the inverted summation symbol is used to denote the summation over the second and, later, third summation indices. In the expansion (3.4) $\hat{P}_k^{(0,m)}(s)$, $k=0,1,2,\cdots$, with $s=2\rho^2-1$ are the Jacobi polynomials of degree k in s with $-1\le s\le 1$, *normalized* so that

$$\frac{1}{4}\int_{-1}^{1}\left(\frac{1+s}{2}\right)^m\hat{P}_k^{(0,m)}(s)\hat{P}_{k'}^{(0,m)}(s)\,ds=\delta_{k,k'},\qquad k,k'=0,1,\cdots. \tag{3.5}$$

A direct calculation leads to

$$\hat{P}_k^{(0,m)}(s)=\sqrt{2(2k+m+1)}\,P_k^{(0,m)}(s),\quad k=0,1,\cdots.$$

We note in passing that the basis functions $\rho^m\,\hat{P}_k^{(0,m)}(2\rho^2-1)$ only differ from those proposed in [15,20] by a scaling factor.

Notice that different expansion functions are used to express how each Fourier component $u_{\pm m}(\rho,\zeta)$ depends on the radial variable ρ. The number of involved functions decreases with m, going from $M+1$, for the first component with $m=0$, to only one, for the last Fourier component with $m=M$. Correspondingly, the array of the expansion coefficients, denoted by

$$U_{\pm m}=\{u_{k;j;\pm m},i=0,1,\cdots,M-m;j=0,1,2,\cdots,J\},$$

will be of dimensions $(M-m+1)\times(J+1)$. The expansion coefficients of the Fourier-spectral representation of the unknowns can be organized in a set of rectangular matrices with variable first dimension, going from the largest size of $M+1$, for $m=0$, to the smallest size of 1 for $m=M$. Note that the variable index m runs only on the nonnegative integers and equations containing $\pm m$ actually represent two sets of relations.

The basis $\hat{L}_j(\zeta)$ used to represent the dependence on the axial variable ζ consists of the *normalized* Legendre polynomials, namely, $\hat{L}_j(\zeta)\equiv\sqrt{j+1/2}\,L_j(\zeta)$, for $j\geq 0$, where $L_j(\zeta)$, $j\geq 0$, are the Legendre polynomials.

By using the Galerkin method, the weak variational formulation of the Helmholtz-Neumann problem yields the following system of linear equations

$$\Big(\frac{1}{c^2}\hat{D}_{\boxed{m}}+\gamma\hat{I}_{\boxed{m}}\Big)\hat{U}_{\pm m}+\hat{U}_{\pm m}\hat{D}\,\frac{1}{H^2}=\hat{G}_{\pm m}+\langle\text{B.I.}\rangle_{\pm m},\tag{3.6}$$

where the "hat" on the matrices indicates that normalized bases of Jacobi polynomials and Legendre polynomials are involved in the definition of the their elements.

The special notation $\boxed{m}$ is adopted to emphasize that the size of the (square) left-multiplying matrices is dependent on index m. The dimension corresponding to $\boxed{m}$ is $M-m+1$, running from $M+1$ for $m=0$ to 1 for $m=M$, as depicted in Fig. 1 for $M=3$.

In the array equation above, the matrix $\hat{I}_{\boxed{m}}$ is the identity matrix of order $M-m+1$ while the matrix $\hat{D}_{\boxed{m}}$ represents the second-order operator associated with the radial variable, namely

$$\begin{aligned}\hat{D}_{\boxed{m}k,k'}=\int_{-1}^{1}\Big\{&4\Big(\frac{1+s}{2}\Big)\frac{d}{ds}\Big[\Big(\frac{1+s}{2}\Big)^{m/2}\hat{P}_k^{(0,m)}(s)\Big]\frac{d}{ds}\Big[\Big(\frac{1+s}{2}\Big)^{m/2}\hat{P}_{k'}^{(0,m)}(s)\Big]\\&+\frac{m^2}{4}\Big(\frac{1+s}{2}\Big)^{m-1}\hat{P}_k^{(0,m)}(s)\,\hat{P}_{k'}^{(0,m)}(s)\Big\}\,ds,\end{aligned}\tag{3.7}$$

with $0\leq(k,k')\leq M-m$. The integration in the radial direction is performed numerically by Gauss-Legendre quadrature with $M+1$ integration points, which are distributed

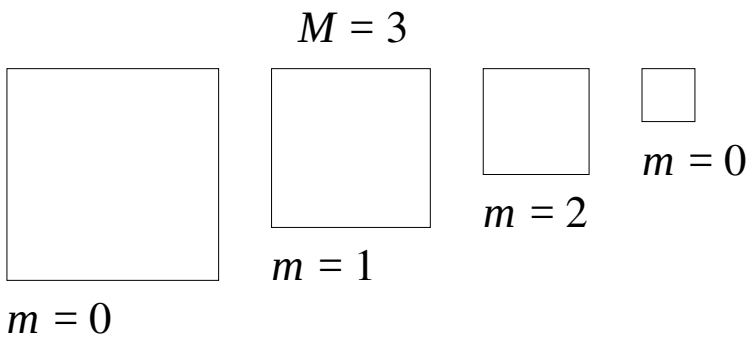

Figure 1: Sketch of the dimension of radial matrices as a function of the Fourier index m.

nearly uniformly in the radial coordinate ρ, near the axis. On the other side, the matrix $\hat{D}$ representing the axial stiffness is defined by

$$\hat{D}_{j,j'} = \int_{-1}^{1} \frac{d\hat{L}_j(\zeta)}{d\zeta} \frac{d\hat{L}_{j'}(\zeta)}{d\zeta} d\zeta. \tag{3.8}$$

The right-hand side is expressed by the sum on the source term

$$\hat{g}_{k;j;\pm m} = \frac{1}{4} \int_{-1}^{1} \int_{-1}^{1} \Big(\frac{1+s}{2}\Big)^{m/2} \hat{P}_k^{(0,m)}(s) f_{\pm m}\big(c\big(\tfrac{1+s}{2}\big)^{1/2}, H\zeta\big) \hat{L}_j(\zeta)\, ds d\zeta \tag{3.9}$$

with the boundary term

$$\begin{aligned}\langle \text{B.I.} \rangle_{k;j;\pm m} = {} & \frac{1}{c} \hat{P}_k^{(0,m)}(1) \int_{-1}^{1} b^{\text{o}}_{\pm m}(H\zeta) \hat{L}_j(\zeta) d\zeta \\ & + \frac{1}{4H} \int_{-1}^{1} \Big(\frac{1+s}{2}\Big)^{m/2} \hat{P}_k^{(0,m)}(s) \big[b^{\text{t}}_{\pm m}\big(c\big(\tfrac{1+s}{2}\big)^{1/2}\big)\big) \hat{L}_j(1) - b^{\text{b}}_{\pm m}\big(c\big(\tfrac{1+s}{2}\big)^{1/2}\big)\big) \hat{L}_j(-1) \big] ds.\end{aligned} \tag{3.10}$$

The linear system (3.6) is solved by double diagonalization. The diagonalization leads to symmetric eigenvalue problems for the matrices $\hat{D}_{\boxed{m}}$, $m = 0,1,\cdots,M$, on the left and $\hat{D}$ on the right and is dealt with by the LAPACK routine `dsyev`.

The L^∞ and L^2_r errors for the solution of the Neumann problem with $\gamma = 1.5$ in the cylinder $r \le 1.5$, $|z| \le 1$ are reported in Table 1 and show the expected spectral convergence.

Table 1: Neumann problem for Helmholtz operator with $\gamma = 1.5$ in the cylinder $r \le 1.5$, $|z| \le 1$. $u = e^{p(x-x_0)^2+q(y-y_0)^2+z-z_0}$, with $p = 0.5, q = 1.2$ and $\boldsymbol{r}_0 = (0.1, 0.2, 0.3)$.

$J = M$	10	15	20	25	30
L^∞ error	8.9×10^{-4}	2.9×10^{-7}	2.0×10^{-10}	5.0×10^{-12}	1.3×10^{-11}
L^2_r error	9.8×10^{-4}	3.6×10^{-7}	2.7×10^{-10}	1.1×10^{-11}	3.7×10^{-11}

4 Dirichlet problem

Despite not being plagued by any centre problem, Matsushima and Marcus basis has two main drawbacks. First, while it is well suited to solve the Neumann problem, it does not accommodate easily Dirichlet boundary conditions since the basis functions are all nonzero on the lateral surface of the cylinder. Second, as is readily seen from Fig. 3, the Helmholtz discrete operator is quite ill conditioned since its condition number grows as M^4, a typical behaviour for collocation spectral methods.

To see how such drawbacks can be overcome, let us start by stating the Dirichlet problem. We assume a Dirichlet condition $u|_{\partial\Omega}=a$ on the boundary $\partial\Omega$ which consists of the lateral cylindrical surface $c\times[-H,H]\times[0,2\pi)$ and of the top and bottom circular lids $(0,c]\times\{\pm H\}\times[0,2\pi)$, so that a represents the value of u prescribed on such a boundary. After introducing the truncated Fourier expansion of the boundary data, we obtain the set of conditions

$$u_m(c,z)=a_m^{\mathrm{o}}(z),\ \ |z|\le H,\qquad u_m(r,\mp H)=a_m^{\mathrm{b,t}}(r),\ \ 0\le r\le c, \tag{4.1}$$

for the modal unknown $u_m(c,z)$. Here $a_{\pm m}^{\mathrm{o}}(z)$, with $|z|\le H$, denotes the Dirichlet data for the Fourier components $\pm m$ on the outer side, while $a_{\pm m}^{\mathrm{b}}(r)$ and $a_{\pm m}^{\mathrm{t}}(r)$, with $0\le r\le c$, denote those on the bottom and top sides.

The approximate solution $u_{\pm m}(\rho,\zeta)$ is expanded in the double series

$$u_{\pm m}(\rho,\zeta)=\sum_{k=0}^{M-m}\rho^m P_k^{\star m}\left(2\rho^2-1\right)u_{k;j;\pm m}\sum_{j=0}^{J}L_j^*(\zeta). \tag{4.2}$$

Here the basis functions $P_k^{\star m}(s)$ are defined in terms of Jacobi polynomials $P_k^{(\alpha,\beta)}(s)$, $-1\le s\le 1$, by the relations:

$$P_0^{\star m}(s)=1\quad\text{and}\quad P_k^{\star m}(s)=\frac{1-s}{2}P_{k-1}^{(1,m)}(s),\ \ k=1,2,\cdots. \tag{4.3}$$

The four sets of basis functions $\rho^m P_k^{\star m}\left(2\rho^2-1\right)$ for $M=3$ are shown in Fig. 2. The figure shows that, for each value of m, only one basis function assumes nonhomogeneous values on the outer radius thus enabling to relieve Dirichlet boundary conditions.

On the other side, the basis $\{L_j^*(\zeta)\}$, $-1\le\zeta\le 1$, is defined as

$$L_0^*(\zeta)=1,\quad L_1^*(\zeta)=\frac{\zeta}{\sqrt{2}},\quad L_n^*(\zeta)=\frac{L_{n-2}(\zeta)-L_n(\zeta)}{\sqrt{2(2n-1)}},\quad n\ge 2. \tag{4.4}$$

This basis is slightly more complicated than the one for the Neumann problem since it contains linear combinations of two Legendre polynomials which vanish on the boundary to satisfy homogeneous Dirichlet conditions, as introduced by Shen [18].

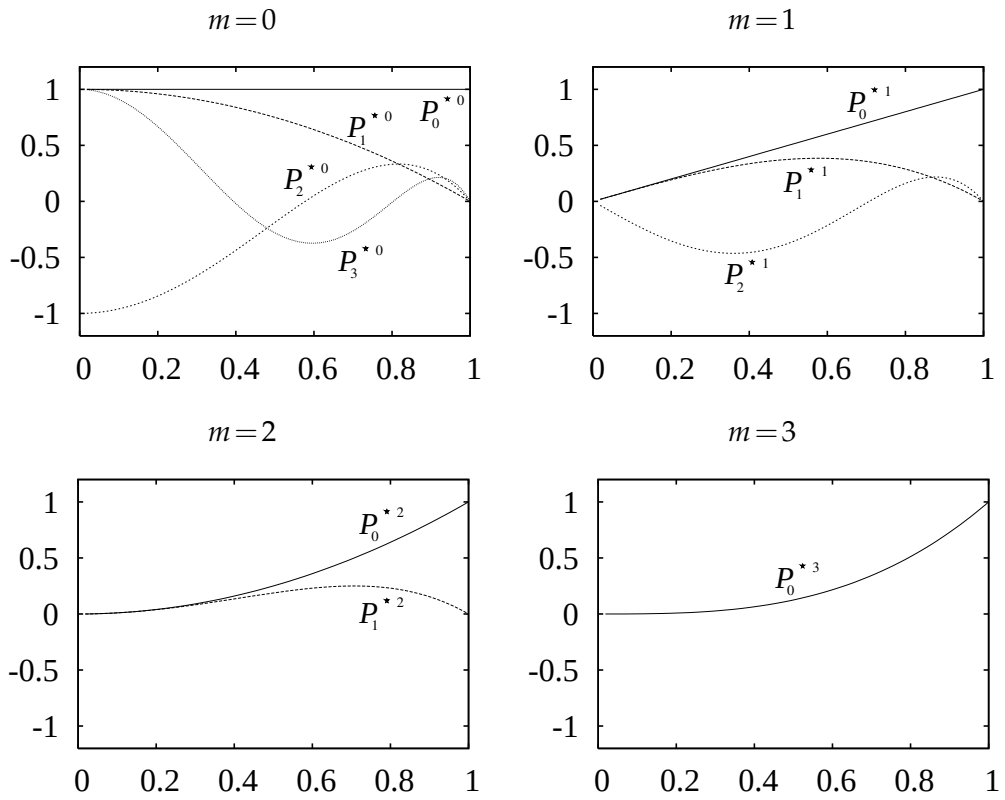

Figure 2: Radial basis functions $\rho^m P_k^{\star m}(2\rho^2-1)$, with $k=0,1,\cdots,M-m$, for the Dirichlet problem: the basis functions belonging to each Fourier subspace are shown for $M=3$.

The complete spectral expansion considered here for the unknown $u(\rho,\zeta,\phi)$ of the elliptic boundary value problem in the cylindrical domain is therefore given by

$$\begin{aligned} u(\rho,\zeta,\phi) = &\sum_{k=0}^{M} P_k^{\star 0}(2\rho^2-1)\, u_{k;j;0}\, L_j^*(\zeta) \sum_{j=0}^{J} \\ &+2\left\{ \sum_{k=0}^{M-m} \rho^m P_k^{\star m}(2\rho^2-1)\, u_{k;j;\pm m}\, L_j^*(\zeta) \sum_{j=0}^{J} \right\} \begin{matrix} \cos(m\phi) \\ -\sin(m\phi) \end{matrix} \sum_{m=1}^{M-1} \\ &+\rho^M \left\{ u_{0,j;M}\, L_j^*(\zeta) \sum_{j=0}^{J} \right\} \cos(M\phi). \end{aligned} \tag{4.5}$$

The presence of superposed cosine and sine functions means that two distinct series are involved by the Fourier summation. The nested dependence of the lower extreme of the first summation on the third index m must be noticed.

Introducing the expansion of $u_m(\rho,\zeta)$ above into the weak equation for this unknown, and choosing as weighting functions $v(\rho,\zeta)$ the same basis functions used to expand the

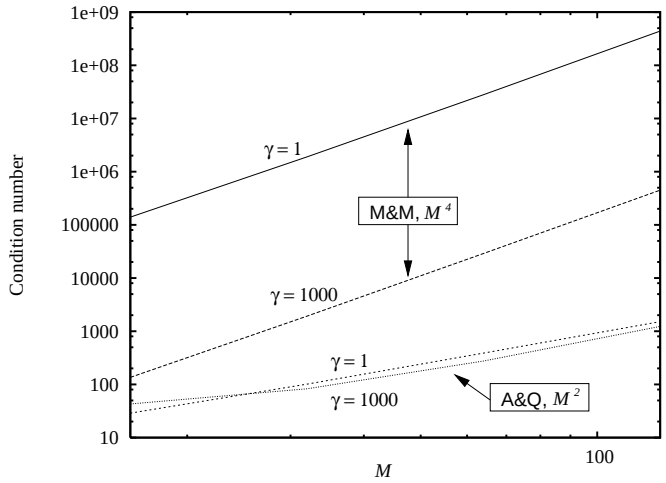

Figure 3: Comparison of the Helmholtz discrete operator condition number for Matsushima and Marcus (M&M) basis versus present basis (A&Q).

solution, the weak equation leads to the following system of equations

$$\Big(\frac{1}{c^2}D_{\boxed{m}}+\gamma M_{\boxed{m}}\Big)U_{\pm m}M+M_{\boxed{m}}U_{\pm m}D\frac{1}{H^2}=G_{\pm m}+\langle \text{B.I.}\rangle_{\pm m}. \tag{4.6}$$

The matrices occurring in this system are defined as follows:

$$\begin{aligned} D_{\boxed{m}k,k'} &= \int_{-1}^{1}\Bigg\{4\Big(\frac{1+s}{2}\Big)\frac{d}{ds}\Bigg[\Big(\frac{1+s}{2}\Big)^{m/2}P_k^{\star m}(s)\Bigg]\frac{d}{ds}\Bigg[\Big(\frac{1+s}{2}\Big)^{m/2}P_{k'}^{\star m}(s)\Bigg] \\ &\quad+\frac{m^2}{4}\Big(\frac{1+s}{2}\Big)^{m-1}P_k^{\star m}(s)P_{k'}^{\star m}(s)\Bigg\}ds, \\ M_{\boxed{m}k,k'} &= \frac{1}{4}\int_{-1}^{1}\Big(\frac{1+s}{2}\Big)^{m}P_k^{\star m}(s)P_{k'}^{\star m}(s)ds, \end{aligned} \tag{4.7}$$

with $0\le(k,k')\le M-m$, for the operators associated with the radial variable r. The matrix $D_{\boxed{m}}$ is diagonal and matrix $M_{\boxed{m}}$ is tridiagonal. These integrals are evaluated numerically by means of Gauss-Legendre quadrature with $M+1$ integration points. The condition number of the matrices $\big(c^{-2}D_{\boxed{m}}+\gamma M_{\boxed{m}}\big)$ is bounded by M^2, see Fig. 3, similarly to condition number of the matrices for Chebyshev approximations proposed by [10]. It compares favourably with the condition number for the analogous matrix computed employing the Matsushima and Marcus basis that grows as M^4, as reported in the same figure.

On the other side, the matrices D and M for the operators in the axial variable are defined by

$$D_{j,j'}=\int_{-1}^{1}\frac{dL_j^*(\zeta)}{d\zeta}\frac{dL_{j'}^*(\zeta)}{d\zeta}d\zeta \quad\text{and}\quad M_{j,j'}=\int_{-1}^{1}L_j^*(\zeta)L_{j'}^*(\zeta)d\zeta. \tag{4.8}$$

The right-hand side is expressed by

$$g_{k;j;\pm m} = \frac{1}{4}\int_{-1}^{1}\int_{-1}^{1}\left(\frac{1+s}{2}\right)^{m/2} P_k^{\star m}(s)\, f_{\pm m}\left(c\left(\tfrac{1+s}{2}\right)^{1/2}, H\zeta\right) L_j^*(\zeta)\, ds\, d\zeta. \tag{4.9}$$

Note that the symbol M representing the right multiplying matrix should not be confused with the upper extreme of the truncated Fourier summation.

4.1 Lifting of the Dirichlet condition

The nonhomogeneous Dirichlet value $a_{\pm m}(\ell)$ is taken into account by means of a lifting, a classical procedure for making the boundary conditions homogeneous. The need of a lifting for developing multidimensional spectral solvers achieving a complete variable separation at the numerical level is described in detail for a 3D rectangular domain in [4]. For the considered problem in a cylindrical domain, the lifting consists in expressing the solution $u_{\pm m}(\rho,\zeta)$ as the sum of three contributions

$$u_{\pm m}(\rho,\zeta) = u_{\pm m,0}(\rho,\zeta) + u^{\mathrm{c}}_{\pm m,a}(\rho,\zeta) + u^{\mathrm{s}}_{\pm m,a}(\rho,\zeta), \tag{4.10}$$

where $u_{\pm m,0}(\rho,\zeta)$ is assumed to satisfy a homogeneous Dirichlet condition. Furthermore, $u^{\mathrm{c}}_{\pm m,a}(\rho,\zeta)$ is the lifting contribution matching the boundary values at the two *circles* of intersection between the lateral surface of the cylinder with its top and bottom sides, while $u^{\mathrm{s}}_{\pm m,a}(\rho,\zeta)$ is the lifting contribution to relieve the nonzero boundary values inside the three aforementioned *surfaces*, and therefore equals $u_{\pm m}(\rho,\zeta) - u^{\mathrm{c}}_{\pm m,a}(\rho,\zeta)$ there.

The contribution $u^{\mathrm{c}}_{\pm m,a}(\rho,\zeta)$ to the lifting is evaluated by collocation, which enables one to satisfy the Dirichlet boundary condition in a strong sense exclusively along the two circles. The second contribution $u^{\mathrm{s}}_{\pm m,a}(\rho,\zeta)$ of the lifting is defined by the Galerkin-Legendre approach, which guarantees the optimality of the approximation (in the L^2_r norm). The combination of these two contributions is finally used to perturb the right-hand side of the discrete elliptic equation to obtain the final system of algebraic equations.

The lifting of nonzero Dirichlet boundary values leads to the following linear system of discrete equations

$$\left(\frac{1}{c^2}D_{\boxed{m}} + \gamma M_{\boxed{m}}\right) U_{\pm m} M + M_{\boxed{m}} U_{\pm m} \frac{1}{H^2} = G_{\pm m},$$

where matrix $G_{\pm m}$ includes the effect of the lifting and where all capital letters in "sans serif" font refer to matrices and arrays associated with the "lifted" problem. Notice that there is a subtlety in the use of the index notation $\boxed{m}$ for the left-multiplying matrices of the lifted problem. The order of these matrices is $M-m$, *i.e.*, one unit less than that of their respective original matrices before the lifting, since the first component is eliminated by the lifting. This implies that in the last problem on the left for $m = M$ these "lifted" left-multiplying matrices will not exist. Thus, the left part of the solution for $m = M$

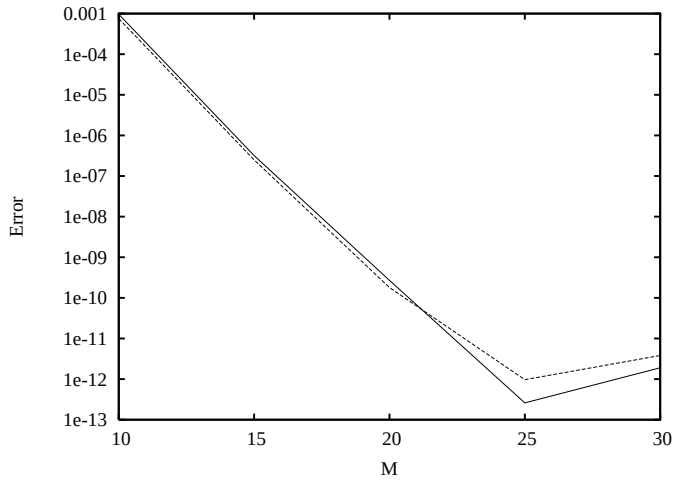

Figure 4: L^2 (solid line) and L^∞ (dashed line) error Dirichlet problem for Helmholtz operator with $\gamma=1.5$ in the cylinder $r\leq 1.5$, $|z|\leq 1$. Exact solution $u=e^{p(x-x_0)^2+q(y-y_0)^2+z-z_0}$, with $p=0.5, q=1.2$ and $\boldsymbol{r}_0=(0.1,0.2,0.3)$.

will consist only in taking into account the boundary values $a^{\mathrm{o}}_{\pm M}(z)$ specified on the cylindrical surface $r=c$. For details see [4].

The linear system is solved by double diagonalization. The diagonalization on the left leads to generalized symmetric eigenvalue problems for the matrix pairs $(D_{\boxed{m}}, M_{\boxed{m}})$, $m=0,1,\cdots,M-1$, and is dealt with by the LAPACK routine `dsygvd`. The diagonalization on the right for banded symmetric matrix M is obtained by `dsbev`.

4.2 Numerical results

The results of the Helmholtz solver with $\gamma=1.5$ for the Dirichlet problem in the cylinder $\Omega=(r\leq 1.5, |z|\leq 1)$ are shown in Fig. 4 and also reported in Table 2 and demonstrate the spectral accuracy of the proposed method.

Table 2: Dirichlet problem for Helmholtz operator with $\gamma=1.5$ in the cylinder $r\leq 1.5$, $|z|\leq 1$. Exact solution $u=e^{p(x-x_0)^2+q(y-y_0)^2+z-z_0}$, with $p=0.5, q=1.2$ and $\boldsymbol{r}_0=(0.1,0.2,0.3)$.

$J=M$	10	15	20	25	30
L^∞ error	7.5×10^{-4}	2.5×10^{-7}	1.8×10^{-10}	9.7×10^{-13}	3.8×10^{-12}
L^2_r error	9.6×10^{-4}	3.2×10^{-7}	2.7×10^{-10}	2.6×10^{-13}	1.9×10^{-12}

The accuracy of the present 3D Dirichlet solver is compared with Shen's solver for polar coordinates on the Poisson problem with exact solution $u(r,\phi)=e^{r(\cos\phi+\sin\phi)}$. The errors of the two solvers given in Table 3 show that Shen's 2D solver is marginally more accurate at low resolution and also more insensitive to roundoff errors.

A nonplanar version of this Poisson problem with a truly 3D solution $u=e^{r(\cos\phi+\sin\phi)+z}$

Table 3: L^2_r error for Poisson-Dirichlet problem in the cylinder $r\leq 1$, $|z|\leq 1$. $u=e^{r(\cos\phi+\sin\phi)}$.

M	8	16	32	64
Present, 3D	4.7×10^{-8}	3.2×10^{-15}	4.7×10^{-15}	2.5×10^{-14}
Shen, 2D [19]	2.6×10^{-8}	1.8×10^{-15}	1.8×10^{-15}	2.7×10^{-15}

Table 4: L^∞ error for Poisson-Dirichlet problem in the cylinder $r\leq 1$, $|z|\leq 0.5$. $u=e^{r(\cos\phi+\sin\phi)+z}$.

$J=M$	8	16	32	64
Present, spectral	4.9×10^{-8}	5.9×10^{-15}	1.4×10^{-14}	9.6×10^{-14}
Fourier/FD [11]	3.4×10^{-3}	9.2×10^{-4}	2.3×10^{-4}	6.0×10^{-5}

in the cylinder $\Omega=(r\leq 1,\ |z|\leq 0.5)$ is then solved to compare the proposed spectral method with the Fourier/finite difference method of Lai et al. [11]. The L^∞ errors of the two algorithms for an equal number of degrees of freedom in the radial and axial directions are given in Table 4. These results show the second-order converge rate of the hybrid method *vis-a-vis* the spectral convergence of the fully spectral method.

5 Vector Dirichlet problem

We consider now the case of a vector elliptic equation, for instance the Helmholtz equation

$$\left(-\nabla^2+\gamma\right)\boldsymbol{u}=\boldsymbol{f}(r,z,\phi)$$

in cylindrical coordinates, with the Laplace operator acting on a vector field defined by

$$\boldsymbol{\nabla}^2=\begin{pmatrix}\nabla^2-\dfrac{1}{r^2} & -\dfrac{2}{r^2}\dfrac{\partial}{\partial\phi} & 0\\ \dfrac{2}{r^2}\dfrac{\partial}{\partial\phi} & \nabla^2-\dfrac{1}{r^2} & 0\\ 0 & 0 & \nabla^2\end{pmatrix},\quad\text{with}\quad \nabla^2=\frac{1}{r}\frac{\partial}{\partial r}\left(r\frac{\partial}{\partial r}\right)+\frac{\partial^2}{\partial z^2}+\frac{1}{r^2}\frac{\partial^2}{\partial\phi^2},\tag{5.1}$$

supplemented by the Dirichlet boundary condition $\boldsymbol{u}_{|\partial\Omega}=\boldsymbol{a}$, where $\boldsymbol{a}$ is defined on the entire boundary $\partial\Omega$ of the cylindrical domain.

The domain of definition of the elliptic equation is assumed to go all around the z-axis, that is, $0\leq\phi<2\pi$. Under these circumstances, since we are interested in purely *real* vector fields, we can represent $\boldsymbol{u}(r,z,\phi)$ by means of a real Fourier expansion, we can write

$$\boldsymbol{u}(r,z,\phi)=\boldsymbol{u}_0(r,z)+2\sum_{m=1}^{\infty}\Big[\boldsymbol{u}_m(r,z)\cos(m\phi)-\boldsymbol{u}_{-m}(r,z)\sin(m\phi)\Big],\tag{5.2}$$

where

$$\boldsymbol{u}_m(r,z;\phi)=u^r_m(r,z)\hat{\boldsymbol{r}}(\phi)+u^\phi_m(r,z)\hat{\boldsymbol{\phi}}(\phi)+u^z_m(r,z)\hat{\boldsymbol{z}},\quad -\infty<m<\infty,\tag{5.3}$$

and the right-hand side is expanded in a similar way.

Let us define, the following partial differential operators

$$\boldsymbol{\partial}_m^2 = \begin{pmatrix} \partial_m^2 - \dfrac{1}{r^2} & \dfrac{2m}{r^2} & 0 \\ \dfrac{2m}{r^2} & \partial_m^2 - \dfrac{1}{r^2} & 0 \\ 0 & 0 & \partial_m^2 \end{pmatrix}, \quad \partial_m^2 = \frac{1}{r}\frac{\partial}{\partial r}\left(r\frac{\partial}{\partial r}\right) - \frac{m^2}{r^2} + \frac{\partial^2}{\partial z^2}, \tag{5.4}$$

for $-\infty < m < \infty$. Introducing the expansions for $\boldsymbol{u}$ and $\boldsymbol{f}$ in the Helmholtz equation and equating similar terms with respect to the angular basis functions, we obtain a series of systems of equations. Each system is uncoupled from the others,

$$(-\boldsymbol{\partial}_m^2 + \gamma) \begin{pmatrix} u_m^r \\ u_{-m}^\phi \\ u_m^z \end{pmatrix} = \begin{pmatrix} f_m^r(r,z) \\ f_{-m}^\phi(r,z) \\ f_m^z(r,z) \end{pmatrix}, \quad -\infty < m < \infty. \tag{5.5}$$

The minus sign in front of m for the ϕ components explains the change of sign of one off-diagonal term in the Fourier transform from (5.1) to (5.4).

For $m=0$ the system consists of three uncoupled equations since the vector differential operator ∂_0^2 is diagonal. For any $|m| \geq 1$ we have a series of systems each consisting of a subsystem of two coupled equations for the radial and angular components of velocity plus an uncoupled equation for the axial component.

5.1 Uncoupling the cylindrical components

The z component of the vector field $\boldsymbol{u}_m$ being uncoupled, we focus our attention on the algorithm for the uncoupled solution of the other two components, namely, we consider the two-component vector unknown

$$\boldsymbol{u}_m(r,z;\phi) = u_m^r(r,z)\,\hat{\boldsymbol{r}}(\phi) + u_m^\phi(r,z)\,\hat{\boldsymbol{\phi}}(\phi), \quad -\infty < m < \infty,$$

for which the system above reduces to

$$(-\boldsymbol{\partial}_m^2 + \gamma) \begin{pmatrix} u_m^r \\ u_{-m}^\phi \end{pmatrix} = \begin{pmatrix} f_m^r(r,z) \\ f_{-m}^\phi(r,z) \end{pmatrix}, \quad \text{where now} \quad \boldsymbol{\partial}_m^2 = \begin{pmatrix} \partial_m^2 - \dfrac{1}{r^2} & \dfrac{2m}{r^2} \\ \dfrac{2m}{r^2} & \partial_m^2 - \dfrac{1}{r^2} \end{pmatrix}. \tag{5.6}$$

Let us introduce the following transformation matrix

$$\mathrm{Q} = \frac{1}{\sqrt{2}} \begin{pmatrix} 1 & 1 \\ 1 & -1 \end{pmatrix}, \tag{5.7}$$

which is symmetric and orthogonal, namely, $\mathbb{Q}^T=\mathbb{Q}^{-1}=\mathbb{Q}$.

By left multiplying the system (5.6) for $m\neq 0$ by $\mathbb{Q}$ and exploiting the properties of $\mathbb{Q}$, we obtain

$$\mathbb{Q}\left(-\partial_m^2+\gamma\right)\mathbb{Q}\,\mathbb{Q}\begin{pmatrix}u_m^r\\ u_{-m}^\phi\end{pmatrix}=\mathbb{Q}\begin{pmatrix}f_m^r(r,z)\\ f_{-m}^\phi(r,z)\end{pmatrix}. \tag{5.8}$$

Since

$$\mathbb{Q}\,\partial_m^2\,\mathbb{Q}=\begin{pmatrix}\partial_{m-1}^2 & 0\\ 0 & \partial_{m+1}^2\end{pmatrix} \tag{5.9}$$

is diagonal, system (5.6) transforms into the two uncoupled equations

$$\left(-\partial_{m-1}^2+\gamma\right)u_{m-1}^1=f_{m-1}^1(r,z);\qquad \left(-\partial_{m+1}^2+\gamma\right)u_{m+1}^2=f_{m+1}^2(r,z), \tag{5.10}$$

where

$$\begin{pmatrix}f_{m-1}^1\\ f_{m+1}^2\end{pmatrix}=\mathbb{Q}\begin{pmatrix}f_m^r\\ f_{-m}^\phi\end{pmatrix}\quad\text{and}\quad\begin{pmatrix}u_m^r\\ u_{-m}^\phi\end{pmatrix}=\mathbb{Q}\begin{pmatrix}u_{m-1}^1\\ u_{m+1}^2\end{pmatrix}. \tag{5.11}$$

The solution algorithm for the vector elliptic equation amounts to the following five steps:

1. transform the right-hand side $\boldsymbol{f}$ and the Dirichlet boundary datum $\boldsymbol{a}$, in the Fourier space,
2. apply the transformation $\mathbb{Q}$ to (the planar part of) all the Fourier components of the source and of the boundary values, except for the constant mode $m=0$,
3. solve the uncoupled equations,
4. apply the inverse of the transformation $\mathbb{Q}$ to all the Fourier components of the solution except for the first mode,
5. antitransform the solution from the Fourier domain to the physical space.

The axial velocity component is uncoupled and is solved independently from the radial-angular component of the field. The Fourier expansion (5.2) is truncated as in the scalar problem, except for the highest wavenumber $\boldsymbol{u}_M=(0,0,u_M^z)$.

5.2 Numerical test

To test the spectral solver for the vector Helmholtz-Dirichlet problem in a cylindrical domain, the exact solution of the vector problem must be constructed so as to be infinitely differentiable also on the cylinder axis. This can be easily done by defining the vector field in terms of its Cartesian components, each one written as a function of the Cartesian

Table 5: Vector Dirichlet problem for Helmholtz operator with $\gamma=1.5$ in the cylinder $r\leq 1.5$ and $|z|\leq 1.5$. The exact solution $\boldsymbol{u}=(u^x,u^y,u^z)(x,y,z)$ defined in the text.

$J=M$	10	15	20	25	30
L^∞ error	2.7×10^{-2}	4.0×10^{-5}	2.3×10^{-8}	1.1×10^{-11}	3.5×10^{-11}
L^2_r error	2.8×10^{-2}	5.2×10^{-5}	2.1×10^{-8}	1.0×10^{-11}	2.0×10^{-11}

coordinates, and then transforming to cylindrical coordinates and components. Therefore, the exact vector solution inside a cylinder will be defined by

$$\begin{aligned} u^x &= e^{p_1(x-x_1)^2+q_1(y-y_1)^2+z-z_1}, \quad p_1=0.5, \quad q_1=1.2, \quad (x_1,y_1,z_1)=(0.1,0.2,0.3);\\ u^y &= e^{p_2(x-x_2)^2+q_2(y-y_2)^2+z-z_2}, \quad p_2=0.7, \quad q_2=1.4, \quad (x_2,y_2,z_2)=(0.2,0.3,0.4);\\ u^z &= e^{p_3(x-x_3)^2+q_3(y-y_3)^2+z-z_3}, \quad p_3=0.9, \quad q_3=1.6, \quad (x_3,y_3,z_3)=(0.3,0.4,0.5). \end{aligned} \tag{5.12}$$

The error is evaluated in the L^2_r norm, which for a vector function is defined by

$$\|\boldsymbol{u}\|^2_{L^2_r}=\|u^r\|^2_{L^2_r}+\|u^\phi\|^2_{L^2_r}+\|u^z\|^2_{L^2_r}. \tag{5.13}$$

The errors of the spectral solutions in the cylinder $\Omega=(r\leq 1.5,|z|\leq 1.5)$ are reported in Table 5 and demonstrate the spectral convergence of the uncoupled vector solver.

6 Conclusions

In this paper Galerkin spectral solvers for scalar and vector Helmholtz equations in a cylindrical domain of finite axial extent have been presented. The ultimate aim of our effort is to build a full set of spectral algorithms suitable for the numerical solution of the incompressible Navier-Stokes equations in a cylinder by means of fractional step projection method, as done for rectangular domains in [3]. This method requires solving at each time step a Poisson equation supplemented by Neumann boundary condition for the pressure and a vector Helmholtz equation supplemented typically by Dirichlet conditions on the entire boundary for the velocity. Two bases have been employed, depending on the kind of conditions to be satisfied on the cylinder boundary. For the Neumann problem, the Jacobi one-sided basis proposed in [15,20] has been adopted, while for the Dirichlet scalar and vector problems a new basis enforcing the essential boundary conditions has been introduced. Nonhomogeneous boundary values are accounted for by means of a general lifting implemented at the discrete level. This makes the Dirichlet spectral solver for the cylinder completely general, much in the same spirit of that developed for the Helmholtz equation inside a prism in [2]. As far as the solution of the vector Dirichlet problem is concerned, an uncoupled algorithm has been implemented which is based on the solution of only real scalar equations and which provides spectrally convergent values of the vector solution on the axis. Note that, as in the work of Verkley for 2D

flows [20], the spectral bases proposed here for the unsteady velocity are free from the severe time step restrictions related to an over resolution near the axis.

References

[1] E. ANDERSON ET AL., *LAPACK*, Third Edition, SIAM, Philadelphia, 1999.

[2] F. AUTERI AND L. QUARTAPELLE, Galerkin–Legendre spectral method for the 3D Helmholtz equation, *J. Comput. Phys.*, **161**, 454–483 (2000).

[3] F. AUTERI AND N. PAROLINI, A mixed-basis spectral projection method, *J. Comput. Phys.*, **175**, 1–23 (2002).

[4] F. AUTERI AND L. QUARTAPELLE, Algorithms for the spectral solution of 3D elliptic problems in finite cylindrical regions, *Scientific Report, DIA SR-06-07*.

[5] C. BERNARDI, M. DAUGE AND Y. MADAY, *Spectral Methods for Axisymmetric Domains*, Elsevier, Paris, 1999.

[6] C. BERNARDI AND Y. MADAY, *Approximations Spectrales des Problèmes aux Limites Elliptiques*, Springer-Verlag, Paris, 1992.

[7] J. P. BOYD, *Chebyshev and Fourier Spectral Methods*, Dover, New York, 2001.

[8] C. CANUTO, M. Y. HUSSAINI, A. QUARTERONI AND T. A. ZANG, *Spectral Methods in Fluid Mechanics*, Springer-Verlag, New York, 1988.

[9] H. CHEN, Y. SU AND B. D. SHIZGAL A direct spectral collocation Poisson solver in polar and cylindrical coordinates. *J. Comput. Phys.*, **160**, 453–469 (2000).

[10] W. HEINRICHS, Improved condition number for spectral methods, *Math. Comp.*, **53**, 103–119 (1989).

[11] M.-C. LAI, W.-W. LIN AND W. WANG, A fast spectral/difference method without pole conditions for Poisson-type equations in cylindrical and spherical geometries, *IMA J. Num. Anal.*, **22**, 537–548 (2002).

[12] H. R. LEWIS AND P. M. BELLAN, Physical constraints on the coefficients of Fourier expansions in cylindrical coordinates, *J. Math. Phys.*, **31**, 2592–2596 (1990).

[13] J. M. LOPEZ AND JIE SHEN, An efficient spectral-projection method for the Navier–Stokes equations in cylindrical geometries. I. Axisymmetric cases, *J. Comput. Phys.*, **139**, 308–326 (1998).

[14] J. M. LOPEZ, F. MARQUES AND JIE SHEN, An efficient spectral-projection method for the Navier–Stokes equations in cylindrical geometries. II. Three-dimensional cases, *J. Comput. Phys.*, **176**, 384–401 (2002).

[15] T. MATSUSHIMA AND P. S. MARCUS, A spectral method for polar coordinates, *J. Comput. Phys.*, **120**, 365–374 (1995).

[16] S. A. ORSZAG AND A. T. PATERA, Secondary instability of wall bounded shear flows, *J. Fluid Mech.*, **128**, 347–385 (1983).

[17] A. QUARTERONI AND A. VALLI, *Numerical Approximation of Partial Differential Equations*, Second Printing, Springer-Verlag, Berlin, 1997.

[18] JIE SHEN, Efficient spectral–Galerkin method. I. Direct solvers of second- and fourth-order equations using Legendre polynomials, *SIAM J. Sci. Comput.*, **15** 1489–1505 (1994).

[19] JIE SHEN, Efficient spectral–Galerkin methods. III. Polar and cylindrical geometries, *SIAM J. Sci. Comput.*, **18**, 74–87 (1997).

[20] W. T. M. VERKLEY, A spectral model for two-dimensional incompressible flow in a circular basin. I. Mathematical formulation, *J. Comput. Phys.*, **136**, 100–114 (1997).